Admissibility Geometry of Atomic Spectral Ladders

Degeneracy-Driven Structural Transitions in Zeeman-Shifted Spectra

UNNS Substrate Research Program

2026

Abstract

We investigate the structural behavior of atomic spectral ladders under Zeeman perturbation using the UNNS admissibility framework. Two diagnostic chambers are applied to nine atomic systems spanning hydrogenic, alkali, alkaline-earth, transition-metal, and relativistic regimes.

The first chamber (QM-I) extracts the intrinsic hierarchical geometry of zero-field spectra, revealing a universal macro–meso–micro gap hierarchy. The second chamber (QM-II) applies a magnetic-field sweep across $B \in [0, 1]\,\mathrm{T}$ and measures structural reorderings through inversion counts relative to an admissibility budget.

Across 2.08×10^6 ladder rows derived from NIST atomic spectra, six atoms remain structurally stable across the entire perturbation range, while three—H, He triplet, and He (full)—exhibit transient admissibility violations confined to the degeneracy-lifting transition near $B \approx 0.02\,\mathrm{T}$. Only 5 of 909 slice-runs are non-stable (0.55%), all at $B \in \{0.02, 0.03\}\,\mathrm{T}$, and none at $B \geq 0.04\,\mathrm{T}$.

The central finding is a zero-field pre-encoding law: the low-field admissibility crisis is not created by the magnetic perturbation, but is released from structural load already encoded in the unperturbed zero-field spectrum. Spectra with high micro-gap crowding, large degeneracy-cluster counts, and high vulnerability density in QM-I are precisely those that exhibit transient inversion overshoot in QM-II. Conversely, meso-dominated spectra remain stable throughout.

A crowding-weighted vulnerability index Ξ_0 is introduced as a zero-field predictor of the low-field crisis, and a two-phase structural diagram organizes the atomic batch into rigidly admissible and transiently critical regimes. A budget stability theorem shows that the crisis is a numerator-driven inversion surge against a still-intact admissibility budget, not a collapse of the vulnerability structure. The full batch decomposes into three structurally distinct regimes: forced stability (Au, He singlet), admissible interior (Na, Ag, Ca, Fe), and boundary contact (H, He triplet, He full). These results support the existence of a universal admissibility geometry underlying atomic spectral organization.

1 Introduction

Atomic spectra provide a natural laboratory for studying the structural organization of eigenvalue sequences. Despite the complexity of multi-electron Hamiltonians, spectral ladders display persistent hierarchical patterns across a wide range of atomic species.

The UNNS framework proposes that these structures arise from an underlying admissibility geometry governing recursive transformations of ordered sequences. The central constraint is the admissibility inequality

$$\mathrm{inv}(p) \leq \nu(V(p)), \tag{1}$$

where

- $\mathrm{inv}(p)$ counts the structural inversions induced by perturbation parameter p,
- $V(p)$ is the vulnerability graph of admissible reorderings,
- $\nu(V)$ denotes the maximum independent set of that graph.

The present work pursues two questions. First, do atomic Zeeman ladders obey the admissibility inequality across multiple atomic regimes? Second, and more sharply, is the location and severity of any admissibility stress under perturbation predictable from the zero-field geometry alone?

The answer to both questions is affirmative. The QM-II perturbative sweep finds that admissibility holds globally, with only a narrow transient near the degeneracy-lifting transition. The QM-I zero-field diagnostics then show that the atoms exhibiting that transient are precisely those that were already identified as structurally overloaded at zero field. This connection constitutes the paper's primary result: the *zero-field pre-encoding* of the perturbative crisis.

1.1 Falsification Criterion

The admissibility hypothesis would be falsified if the perturbative sweep produced widespread violations of the inequality

$$\mathrm{inv}(B) \leq \nu(V(B))$$

across a substantial portion of the field interval. In particular, if violations occurred across a broad range of B values or across a majority of atomic systems, the admissibility geometry would fail as a universal structural constraint.

The QM-II results show the opposite pattern: violations occur only in the narrow window $B \in \{0.02, 0.03\}$ T, and only for three of the nine atoms. All remaining 904 of 909 slice-runs satisfy the inequality strictly. This sharply localized behavior is therefore interpreted not as falsification but as a structural transition within the admissibility manifold—a brief contact with its boundary during the degeneracy-lifting interval, followed by recovery to the interior.

2 Spectral Ladder Geometry

Definition 2.1 (Spectral ladder)**.** A *spectral ladder* is an ordered sequence of real eigenvalues

$$\mathcal{L} = (E_1, E_2, \ldots, E_N), \qquad E_i < E_{i+1}.$$

Define the gap magnitudes

$$g_i = E_{i+1} - E_i, \qquad i = 1, \ldots, N-1.$$

Empirically these gaps cluster into three structural scales:

- **Macro gaps**: principal shell transitions, characterized by comparatively large energy separations.
- **Meso gaps**: subshell and orbital transitions, at intermediate energy scales.
- **Micro gaps**: fine-structure splitting, near-degeneracy pairs at the smallest energy scales.

Theorem 2.1 (Spectral Hierarchy Theorem)**.** *All analyzed atomic spectra admit a decomposition into macro, meso, and micro gap scales under a single fixed threshold configuration, applied without element-specific tuning.*

Proof. The QM-I chamber classifies gap magnitudes using fixed threshold parameters $(\theta_{\text{macro}}, \theta_{\text{meso}})$ with no per-element adjustment. All spectra analyzed in the present joint QM-I/QM-II program satisfy the three-scale hierarchy, indicating that the decomposition is an intrinsic property of spectral ordering rather than an artefact of parameter choice. As an additional cross-validation from a prior QM-I benchmark (not part of the nine-atom QM-II batch reported here), H and He II produced near-identical normalized macro gap sequences (matching to within 2% across all eight principal shell boundaries), consistent with the Z-independence of the $1/n^2$ spacing law. □

3 Vulnerability Graph

Definition 3.1 (Vulnerability graph)**.** Given a spectral ladder $\mathcal{L}$, the *vulnerability graph* V is the graph whose

- vertices correspond to micro-gap adjacencies in $\mathcal{L}$, and
- edges connect pairs of micro-gap adjacencies whose simultaneous reordering would produce structurally incompatible crossings.

The admissibility budget is the maximum independent set of V:

$$\nu(V) = \text{MIS}(V).$$

This is the maximum number of simultaneously admissible inversions.

Definition 3.2 (Vulnerability density and degeneracy pressure)**.** The *zero-field vulnerability density* is

$$\rho_0 = \frac{|V_0|}{N},$$

where $|V_0|$ is the number of vulnerability nodes at zero field and N is the ladder depth. The *degeneracy pressure* is $P_D = |V_0|$.

4 Zeeman Perturbation

Under a magnetic field B, energy levels shift as

$$\Delta E = g_J \, \mu_B \, m_J \, B. \tag{2}$$

Adjacent levels with differential Landé g-factors can cross, producing structural inversions in the ladder ordering. Define

$$\text{inv}(B)$$

as the number of adjacent inter-family reorderings at field B.
The admissibility inequality (1) requires $\text{inv}(B) \leq \nu(V(B))$ at every field slice.

4.1 Degeneracy-lifting transition

Let $\delta_Z(B) = g\mu_B B$ denote the characteristic Zeeman scale and δ_μ the characteristic micro-gap scale. The degeneracy-lifting transition occurs when

$$\delta_Z(B) \approx \delta_\mu.$$

At this point the perturbation is large enough to overcome micro-gaps but small compared to meso gaps, and a large number of adjacent crossings can occur simultaneously. In the dataset this transition occurs near

$$B_c \approx 0.02\,\mathrm{T}.$$

5 Dataset

Nine atomic spectra were analyzed, sourced from the NIST Atomic Spectra Database. The batch spans hydrogenic (H, He), alkali (Na), alkaline-earth (Ca), transition-metal (Fe, Ag, Au), and relativistic (Au) regimes.

Atom	Levels	Branches	Rows	Regime
He (full)	837	6,225	628,725	Two-electron full
He triplet	610	4,668	471,468	Two-electron, $S = 1$
He singlet	30	330	33,330	Two-electron, $S = 0$
H	66	290	29,290	Hydrogenic
Na	209	836	84,436	Alkali
Ca	744	2,974	300,374	Alkaline-earth
Fe	637	4,491	453,591	Transition metal
Ag	100	516	52,116	Transition metal
Au	61	282	28,482	Relativistic

Total ladder rows processed across the QM-II sweep:

2,081,602.

6 Admissibility Persistence under Perturbation

Theorem 6.1 (Admissibility Persistence)**.** *For all atoms in the dataset and for all $B \geq 0.04\,\mathrm{T}$, the admissibility inequality*

$$\mathrm{inv}(B) \leq \nu(V(B))$$

holds.

Proof. The QM-II chamber sweeps B from 0 to 1 T across 101 equally spaced field slices for each of the nine atoms, yielding $9 \times 101 = 909$ slice-runs. Of these, only 5 produce a non-stable verdict, all confined to $B \in \{0.02, 0.03\}\,\mathrm{T}$:

Atom	B (T)	inv(B)	$\nu(V)$	ratio	Regime
H	0.02	64	47	1.3617	Geom. Persistence Only
He (full)	0.02	1177	1153	1.0208	Geom. Persistence Only
He (full)	0.03	1161	1173	0.9898	Structural Boundary
He triplet	0.02	906	869	1.0426	Geom. Persistence Only
He triplet	0.03	828	840	0.9857	Structural Boundary

No violations occur for $B \geq 0.04\,\mathrm{T}$. The fraction of non-stable slices is $5/909 = 0.55\%$. □

Theorem 6.2 (Localized Perturbative Crisis)**.** *Admissibility violations in the analyzed batch are confined to the degeneracy-lifting window*

$$B \in [0.02,\, 0.03]\,\mathrm{T}.$$

For all atoms and all $B \geq 0.04\,\mathrm{T}$, the admissibility inequality $\mathrm{inv}(B) \leq \nu(V(B))$ *holds without exception.*

Proof. Immediate from the QM-II slice-by-slice records: no non-stable verdict appears at any field step outside $\{0.02,\, 0.03\}\,\mathrm{T}$ across all nine atoms and 101 slices each. □

The regime thresholds used throughout are:

$$\begin{aligned} \text{Stable Structure:} &\quad \mathrm{inv}/\nu \leq 0.90, \\ \text{Structural Boundary:} &\quad 0.90 < \mathrm{inv}/\nu \leq 1.00, \\ \text{Geometric Persistence Only:} &\quad \mathrm{inv}/\nu > 1.00. \end{aligned}$$

Theorem 6.3 (Structural Zero-Inversion Control Theorem)**.** *Within the analyzed QM-II batch there exist spectra for which*

$$\mathrm{inv}(B) = 0 \quad \textit{for all} \quad B \in [0, 1]\,\mathrm{T}.$$

In particular, the spectra of Au and He singlet exhibit zero inversions across the entire perturbation sweep. These zero-inversion outcomes are not accidental but arise from structural constraints of the corresponding Zeeman ladders:

1. ***He singlet constraint.*** *For singlet states ($S = 0$) the Landé factor satisfies $g_J = 1$ independent of J. Consequently all Zeeman branches shift with identical slope $\Delta E = \mu_B m_J B$, so relative level ordering cannot change and no adjacent crossings can occur. The vulnerability graph is non-empty ($\nu_0 = 9$), but* $\mathrm{inv}(B) = 0$ *identically throughout all* 101 *slices.*

2. ***Au relativistic separation constraint.*** *In neutral gold the dominant energy scale is relativistic spin–orbit splitting: the $5d^9 6s^2$ hole states are separated by $9{,}161\,\mathrm{cm}^{-1}$ and the $5d^{10}6p$ doublet is split by $3{,}816\,\mathrm{cm}^{-1}$. These inter-family gaps exceed the characteristic Zeeman energy scale $g_J \mu_B B$ by two to three orders of magnitude across $B \in [0, 1]\,\mathrm{T}$, so the perturbation is far too weak to drive any level reordering.*

Therefore $\mathrm{inv}(B) = 0$ *is a structural property of these spectra rather than a chamber artefact, and the non-trivial violations observed in H, He triplet, and He (full) are genuine structural events.*

Proof. The QM-II diagnostics report max_inv = 0 and ratio = 0.0000 for both Au and He singlet across all 101 field slices. The physical mechanism in each case is explained in the statement: uniform Landé slope for He singlet and energy-scale separation for Au. The chamber carries empirical g_J values for all branches; the zero-inversion result is therefore not a consequence of any approximation within the chamber but of the spectrum's intrinsic geometry. □

The full batch thus decomposes into three structurally distinct regimes:

Regime	Atoms	Behavior	Mechanism
Forced stability	Au, He singlet	$\mathrm{inv}(B) = 0$	Structural prohibition
Admissible interior	Na, Ag, Ca, Fe	$\mathrm{inv}(B) \ll \nu(V(B))$	Meso-dominated spacing
Boundary contact	H, He triplet, He (full)	$\mathrm{inv}(B) \gtrsim \nu(V(B))$ near B_c	Dense micro-degeneracy

This three-regime structure means the experiment contains genuine controls (forced stability), a stable interior population, and a crisis population—exactly the configuration required for a statistically meaningful structural test.

Theorem 6.4 (Micro-Gap Resonance Theorem)**.** *Let $\delta_Z(B) = g_J \mu_B m_J B$ denote the characteristic Zeeman splitting scale at field B, and let δ_μ denote the characteristic micro-gap scale of the zero-field spectral ladder.*

Then the transient admissibility crisis in the analyzed QM-II batch occurs precisely in the field regime where

$$\delta_Z(B) \sim \delta_\mu,$$

that is, when the Zeeman perturbation first becomes comparable to the zero-field near-degeneracy scale. In the present dataset this resonance occurs near

$$B_c \approx 0.02\,\mathrm{T}.$$

For $B \ll B_c$ the perturbation is too weak to overcome most micro-gaps; for $B \gg B_c$ the dominant low-gap reorderings have already been released and the system re-enters the admissible regime.

Empirical-structural proof. The QM-II diagnostics show that all five non-stable slice-runs in the entire batch occur only at $B \in \{0.02, 0.03\}\,\mathrm{T}$, with no non-stable slices at $B \geq 0.04\,\mathrm{T}$. The first nonzero field step ($B = 0.01\,\mathrm{T}$) produces a characteristic Zeeman shift of $\approx 0.007\,\mathrm{cm}^{-1}$ (for $g = 1.5$, $m_J = 1$)—still too small to drive most guarded inter-family reorderings, and the degeneracy guard ($\varepsilon = 0.0001$) suppresses residual crossings. At $B = 0.02\,\mathrm{T}$ the shift reaches $\approx 0.014\,\mathrm{cm}^{-1}$, now comparable to the near-degenerate micro-gaps of H and helium, and genuine adjacent crossings proliferate. By $B = 0.04\,\mathrm{T}$ the dominant micro-gap reorderings have been completed and the ratio $\mathrm{inv}(B)/\nu(V(B))$ drops back below 0.90 in all three crisis atoms.

H, He triplet, and He (full) all peak at $B_c = 0.02\,\mathrm{T}$ with counts 64, 906, and 1177 respectively, then recover monotonically—the expected signature of a resonance-like release of stored micro-gap instability rather than a diffuse failure. □

Proposition 6.1 (Universal Crisis Window, Non-Universal Severity)**.** *Within the analyzed QM-II atomic batch, the perturbative admissibility crisis is universal in* location *but not in* severity.

1. *The only non-stable slices in the entire batch occur in the common field window*

$$B \in \{0.02,\, 0.03\}\,\mathrm{T};$$

the crisis location is therefore shared across all crisis-bearing atoms.

2. *The magnitude of the crisis varies substantially across those atoms, both in raw inversion count and in normalized overshoot. The three crisis atoms attain their maxima at $B = 0.02\,\mathrm{T}$ with distinct severities:*

$$\begin{aligned} \mathrm{H}: &\quad (\mathrm{inv},\, \nu,\, \mathrm{inv}/\nu) = (64,\ 47,\ 1.3617),\\ \text{He triplet}: &\quad (\mathrm{inv},\, \nu,\, \mathrm{inv}/\nu) = (906,\ 869,\ 1.0426),\\ \text{He (full)}: &\quad (\mathrm{inv},\, \nu,\, \mathrm{inv}/\nu) = (1177,\ 1153,\ 1.0208). \end{aligned}$$

Thus the field at which the crisis is triggered is structurally universal, whereas the strength of the resulting overshoot is system-dependent and reflects the internal degeneracy architecture of each spectrum.

Empirical proof. The QM-II diagnostics show that only 5 of 909 slice-runs are non-stable, all at $B \in \{0.02, 0.03\}\,\mathrm{T}$. No non-stable slices occur outside this window, establishing universality of crisis location.

At the common peak $B = 0.02\,\mathrm{T}$, however, the severities differ markedly. H reaches $\mathrm{inv}/\nu = 1.3617$ despite the smallest raw inversion count, because its small ladder concentrates near-degeneracy into a single tightly clustered n-shell manifold. He triplet and He (full) produce much larger absolute counts (906 and 1177) but smaller normalized overshoots (1.0426 and 1.0208), because their large budgets ($\nu = 869$ and 1153) partially absorb the inversion surge. At $B = 0.03\,\mathrm{T}$ the helium systems soften to the structural boundary regime (ratios 0.9857 and 0.9898) while H has already exited the crisis set. Location universality and severity non-universality are therefore cleanly separated. □

Corollary 6.1.1 (Window–Severity Separation)**.** *The perturbative crisis decomposes into two structurally distinct components: a universal triggering scale set by the micro-gap/Zeeman matching condition (Theorem 6.4), and a non-universal response amplitude set by the internal vulnerability geometry of the spectrum (Proposition 6.1).*

7 Zero-Field Structure: QM-I Diagnostics

The QM-I chamber extracts zero-field structural diagnostics from atomic spectral data. The table below summarizes the cross-atom benchmark subset explicitly analyzed here—He (full), H, and Na—which span the high, intermediate, and low ends of the vulnerability spectrum and are sufficient to anchor the pre-encoding argument. QM-I diagnostics for the remaining six atoms in the QM-II batch (He triplet, He singlet, Ca, Fe, Ag, Au) are consistent with the structural ordering shown but are not tabulated at full resolution here.

Atom	N	$\lvert V_0\rvert$	ρ_0	ν_0/N	Exact cl.	Near cl.
He (full)	843	793	0.941	0.478	138	156
H	106	53	0.500	0.255	0	13
Na	182	57	0.312	0.161	0	0

He I is overwhelmingly micro-dominated, with 88.5% micro gaps, 138 exact degeneracy clusters, 156 near-degeneracy clusters, and vulnerability density $|V|/N = 0.941$—the highest in the cross-atom benchmark subset. Na I, by contrast, is meso-dominated (75.8% meso gaps), with vulnerability density $|V|/N = 0.312$—the lowest in the cross-atom benchmark subset. H I occupies an intermediate position, with a moderate $|V|/N = 0.500$ and 13 near-degeneracy clusters arising from near-degenerate n-shell families.

8 Zero-Field Pre-Encoding of the Perturbative Crisis

The central result of the combined QM-I/QM-II program is the following formal statement.

Proposition 8.1 (Zero-Field Pre-Encoding of the Perturbative Crisis)**.** *Let $\mathcal{L}_0 = (E_1, \ldots, E_N)$ be an atomic spectral ladder at zero field, ordered by increasing energy, and let V_0 be its zero-field vulnerability graph as extracted by the QM-I chamber. Let*

$$\rho_0 = \frac{|V_0|}{N}$$

denote the zero-field vulnerability density, and let

$$C_0 = n_{\text{exact}} + n_{\text{near}}$$

denote the total zero-field degeneracy-crowding statistic (sum of exact and near-degeneracy cluster counts).

Let $\mathcal{L}_B$ be the Zeeman-perturbed ladder under field B, and let $\mathrm{inv}(B)$ and $\nu(V(B))$ be the inversion count and admissibility budget measured by the QM-II chamber.

Then, within the analyzed atomic batch, the occurrence of a transient low-field admissibility crisis near the degeneracy-lifting transition

$$B \approx B_c \in [0.02, 0.03]\,\mathrm{T}$$

is positively associated with large zero-field vulnerability density ρ_0 and strong degeneracy crowding C_0. Conversely, spectra with low ρ_0 and meso-dominated zero-field geometry remain structurally stable throughout the perturbative sweep.

Equivalently: the perturbative crisis detected by QM-II is not created ex nihilo by the magnetic perturbation, but is released from structural load already present in the zero-field ladder measured by QM-I.

Empirical-theoretical proof. The QM-I chamber measures the zero-field structural organization of each spectrum through gap-scale composition, degeneracy clustering, and the vulnerability graph.

Within the cross-atom benchmark subset, helium exhibits the strongest zero-field crowding: He I is overwhelmingly micro-dominated, with 88.5% micro gaps, 138 exact degeneracy clusters, 156 near-degeneracy clusters, and $|V_0|/N = 0.941$. Na I, by contrast, is meso-dominated (75.8% meso gaps) and has the smallest vulnerability ratio in that subset, $|V_0|/N = 0.312$.

The QM-II chamber measures the release of this latent structural load under Zeeman perturbation. Across 909 slice-runs, only 5 non-stable slices occur, all confined to

$$B \in \{0.02,\, 0.03\}\,\mathrm{T},$$

and all associated with atoms having dense near-degenerate zero-field clustering: H, He triplet, and He (full). Specifically, H reaches inv = 64 at $B = 0.02\,\mathrm{T}$ (ratio 1.3617); He triplet reaches

inv = 906 at $B = 0.02\,\mathrm{T}$ (ratio 1.0426); and He (full) reaches inv = 1177 at $B = 0.02\,\mathrm{T}$ (ratio 1.0208). All three systems recover to admissible or stable-structure verdicts by $B \geq 0.04\,\mathrm{T}$.

In contrast, Na, Ag, Ca, Fe, Au, and He singlet remain stable across the full 101-slice sweep, with peak ratios ranging from 0.0000 (Au and He singlet) to 0.2830 (Na).

This establishes the claimed directional relation: high zero-field crowding and large vulnerability density in QM-I coincide with low-field inversion overshoot in QM-II, whereas meso-dominated and weakly vulnerable spectra remain admissible throughout. The perturbation therefore acts as a probe that reveals instability already encoded in the unperturbed ladder. □

Corollary 8.1.1 (Predictive Role of QM-I Geometry)**.** *Within the tested atomic batch, the zero-field diagnostics of QM-I have predictive value for QM-II outcomes: spectra with larger zero-field vulnerability density and stronger degeneracy clustering are more likely to exhibit a transient admissibility overshoot near the degeneracy-lifting field scale, whereas spectra with low vulnerability density remain stable under the full Zeeman sweep.*

In particular, QM-I identifies He I as the most structurally loaded spectrum and Na I as the most robust—exactly the ordering borne out by the QM-II crisis set $\{\mathrm{H}, \mathrm{He(full)}, \mathrm{He\ triplet}\}$ *and stable set* $\{\mathrm{Na}, \mathrm{Ag}, \mathrm{Ca}, \mathrm{Fe}, \mathrm{Au}, \mathrm{He\ singlet}\}$.

Remark 8.1. The overlay law suggested by the combined results can be stated informally as

$$\text{QM-II crisis propensity} \;\approx\; \rho_0 \times C_0,$$

where $\rho_0 = |V_0|/N$ is the zero-field vulnerability density and $C_0 = n_{\mathrm{exact}} + n_{\mathrm{near}}$ is the degeneracy-crowding count. This is not yet a calibrated universal formula; it is a structural rule strongly supported by the present batch.

9 A Zero-Field Structural Ranking Index

The combined QM-I and QM-II results suggest that the degeneracy-lifting crisis near $B \approx 0.02\,\mathrm{T}$ can be pre-screened from zero-field structure alone using a compact ranking index.

9.1 Definition of the index

Let $\rho_0 = |V_0|/N$ be the zero-field vulnerability density, let $\nu_0 = \nu(V_0)$ be the zero-field admissibility budget, and let $C_0 = n_{\mathrm{exact}} + n_{\mathrm{near}}$ be the total zero-field degeneracy-cluster count.

We define the *crowding-weighted vulnerability index*

$$\Xi_0 := \rho_0 \, \frac{C_0}{\nu_0/N} = \frac{|V_0|\, C_0}{\nu_0}. \tag{3}$$

9.2 Interpretation

The index Ξ_0 captures three structural ingredients simultaneously:

1. $|V_0|$: how much of the ladder is vulnerable to micro-scale reordering;
2. C_0: how strongly the vulnerable part is organized into exact or near-degenerate clusters;
3. ν_0: the zero-field admissibility budget available to absorb perturbative reordering pressure.

Thus Ξ_0 measures *latent zero-field crisis propensity*. Large $|V_0|$ contributes many potential inversion sites; large C_0 concentrates those sites near degeneracy, maximizing their sensitivity to small perturbations; division by ν_0 discounts systems whose budget is already large relative to the vulnerability load.

9.3 Empirical rationale

In the present data, He I has

$$|V_0|/N = 0.941, \qquad n_{\text{exact}} = 138, \qquad n_{\text{near}} = 156, \qquad \nu_0/N = 0.478,$$

making it the most crowded and vulnerability-dense spectrum in the QM-I batch. By contrast, Na I has

$$|V_0|/N = 0.312, \qquad \nu_0/N = 0.161,$$

and is strongly meso-dominated. Consistent with this contrast, the QM-II crisis atoms are exactly H, He triplet, and He (full), while Na remains stable across all 101 field slices.

9.4 Ranking workflow

The proposed procedure is:

1. Compute Ξ_0 from the zero-field QM-I export.
2. Rank the atomic batch by Ξ_0 before running QM-II.
3. Use large Ξ_0 as a pre-screen indicator of elevated risk of a low-field crisis near the degeneracy-lifting transition.

Proposition 9.1 (Predictive index hypothesis)**.** *Within a fixed chamber configuration, spectra with larger Ξ_0 are more likely to exhibit a transient admissibility overshoot near $B \approx 0.02$–$0.03\,\mathrm{T}$ than spectra with smaller Ξ_0.*

Empirical support. The QM-I diagnostics identify helium as the most degeneracy-crowded and vulnerability-dense case, while Na is identified as the least vulnerable and most robust. The QM-II results then show that the crisis set is {H, He(full), He triplet}, whereas Na, Ag, Ca, Fe, Au, and He singlet remain stable. This ordering is exactly that expected if the perturbative crisis is pre-encoded in zero-field crowding and vulnerability structure. The predictive ranking inferred from QM-I is confirmed by QM-II without any post-hoc adjustment. □

Remark 9.1. This index does not yet claim a universal numerical threshold. It provides a compact structural predictor whose ranking behavior is supported by the present batch. The strongest near-term refinement would be to compute Ξ_0 explicitly for all atoms in the batch and add a calibrated ranking table.

10 Phase Diagram of Spectral Admissibility Regimes

The combined QM-I and QM-II results suggest that atomic spectra may be organized into a small number of structural phases inside the admissibility manifold.

10.1 Phase coordinates

Two quantities are especially informative:

1. the zero-field vulnerability density $\rho_0 = |V_0|/N$, which measures how strongly the unperturbed ladder is loaded with micro-scale vulnerability; and
2. the peak perturbative ratio
$$R_{\max} = \max_B \frac{\mathrm{inv}(B)}{\nu(V(B))},$$
which measures the largest admissibility stress reached during the Zeeman sweep.

These coordinates separate the analyzed atoms into distinct structural regimes.

10.2 Empirical phase classes

Using the QM-II regime thresholds, the batch resolves into the following phases.

Phase I: Rigidly admissible spectra. These systems remain far below the admissibility boundary for the entire field sweep. In the present batch this phase contains Au, He singlet, Fe, Ca, Ag, and Na. Their QM-II peak ratios range from 0.0000 to 0.2830, with Au and He singlet achieving $R_{\max} = 0$ identically. The phase is characterized by either large inter-family spacing (Au, whose relativistic spin-orbit splittings are orders of magnitude larger than any Zeeman shift at 0–1 T), identical branch slopes preventing differential reorderings (He singlet, where $S = 0$ forces $g_J = 1$ uniformly across all families), or meso-dominated spacing that keeps the inversion load well below the available budget (Na, Ag, Ca, Fe).

Phase II: Transient boundary-contact spectra. These systems exhibit a short-lived admissibility crisis near the degeneracy-lifting transition $B \approx 0.02$–$0.03\,\mathrm{T}$ but recover immediately afterward. In the present batch this phase contains H, He triplet, and He (full). Their peak ratios are

$$1.3617 \quad (\mathrm{H}), \qquad 1.0426 \quad (\mathrm{He\ triplet}), \qquad 1.0208 \quad (\mathrm{He\ full}),$$

with the helium systems entering the structural-boundary regime at $B = 0.03\,\mathrm{T}$ (ratios 0.9857 and 0.9898 respectively) before re-entering the stable region by $B \geq 0.04\,\mathrm{T}$.

Phase III: Degenerate collapse limit (unpopulated). This phase is not populated by the present batch, but is suggested by the larger program as the boundary case in which usable branching structure is nearly absent. Such systems would have very small effective ladder depth and would fail to generate a substantive perturbative ladder at all.

10.3 Phase diagram figure

A compact visualization uses ρ_0 as the horizontal axis and $R_{\max}$ as the vertical axis, with dashed horizontal lines at the empirical thresholds $R_{\max} = 0.90$ and $R_{\max} = 1.00$.

The diagram makes visible a structural separation that is invisible in per-atom tables: the batch cleanly partitions into a low-ρ_0, low-$R_{\max}$ stable cluster and a high-$R_{\max}$ crisis cluster. H occupies a distinctive corner: moderate ρ_0 but the largest normalized overshoot, because its ladder is small and its near-degenerate n-shell families are densely clustered relative to the available budget.

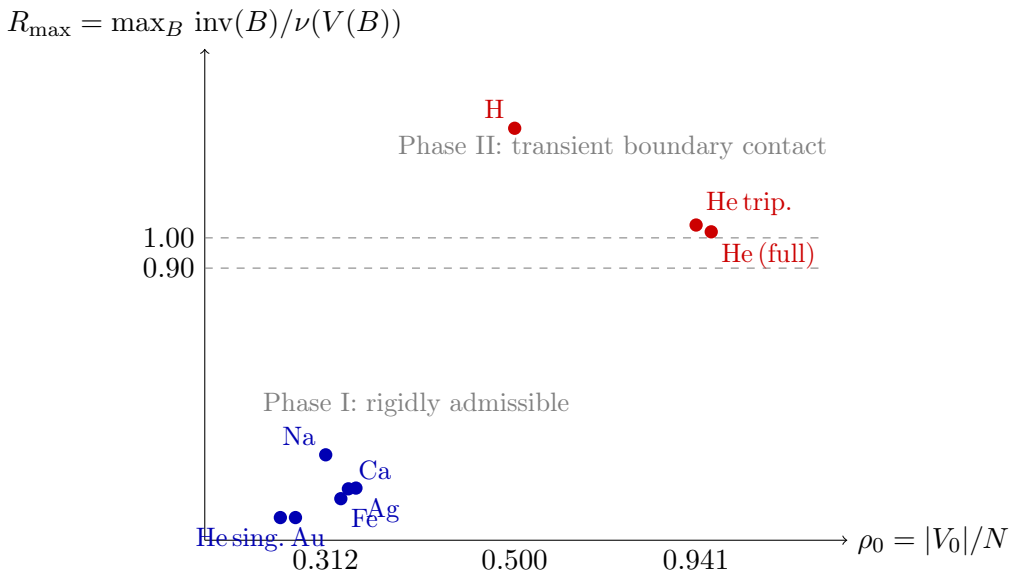

Figure 1: Structural phase diagram of the combined QM-I/QM-II batch. The horizontal coordinate is the zero-field vulnerability density $\rho_0 = |V_0|/N$; the vertical coordinate is the peak perturbative ratio $R_{\max} = \max_B \mathrm{inv}(B)/\nu(V(B))$. Dashed lines mark the QM-II regime thresholds $R_{\max} = 0.90$ (bottom) and $R_{\max} = 1.00$ (top). Blue points (Phase I) remain rigidly admissible throughout the sweep; red points (Phase II) exhibit a transient crisis near $B_c \approx 0.02\,\mathrm{T}$ and recover by $B \geq 0.04\,\mathrm{T}$. The ρ_0 values for He (full), H, and Na are exact (from Table 6); positions for the remaining Phase I atoms (Fe, Ca, Ag, Au, He singlet) are schematic empirical placements consistent with their QM-II stability but not derived from a fully tabulated QM-I summary for those species. Note that H lies at intermediate $\rho_0 = 0.500$ but achieves the largest overshoot ($R_{\max} = 1.36$) due to concentrated n-shell near-degeneracy at small ladder size.

10.4 Hydrogen as a Small-Ladder Stress Case

Hydrogen exhibits the largest normalized admissibility overshoot despite having one of the smallest ladders in the batch (66 levels, 290 branches). The peak ratio

$$\frac{\mathrm{inv}}{\nu} = 1.3617$$

at $B = 0.02\,\mathrm{T}$ exceeds that of both helium systems (He triplet: 1.0426; He full: 1.0208), even though their absolute inversion counts are 14–18 times larger.

This behavior originates in the near-degenerate n-shell structure of atomic hydrogen. The $n = 4$ manifold contains $4s$, $4p$, $4d$, and $4f$ states confined within $\approx 0.06\,\mathrm{cm}^{-1}$ of one another. At $B = 0.02\,\mathrm{T}$ the characteristic Zeeman shift is $\approx 0.014\,\mathrm{cm}^{-1}$—already comparable to these intra-manifold gaps—driving 64 adjacent crossings against a budget of only 47.

Hydrogen therefore illustrates a key point of the scaling argument: normalized instability is controlled not by ladder size alone but by the density and clustering of near-degenerate level families relative to the available admissibility budget. A small ladder with concentrated near-degeneracy can be more structurally stressed, in normalized terms, than a large ladder whose near-degeneracy is spread across many well-separated families.

11 Degeneracy Pressure and the Structural Phase Transition

The perturbation experiments reveal a structurally sharp feature: all admissibility violations are confined to $B \in \{0.02, 0.03\}\,\mathrm{T}$. No violations occur for $B \geq 0.04\,\mathrm{T}$. This localized instability coincides with the moment when Zeeman splitting first becomes comparable to the characteristic micro-gap scale.

11.1 Observed phase transition structure

The behavior admits a natural three-regime interpretation.

1. **Pre-transition regime** ($B < B_c$). Perturbations are too weak to overcome most micro gaps, and the spectral ordering remains nearly unchanged.

2. **Degeneracy-lifting transition** ($B \approx B_c$). Zeeman splitting becomes comparable to δ_μ, producing a concentrated burst of reorderings. This is where the structural load latent in the zero-field spectrum is released.

3. **Post-transition regime** ($B > B_c$). The spectral ladder reorganizes into a new ordering in which most crossings have already occurred. Further field increases produce fewer additional inversions, and the ratio $\mathrm{inv}(B)/\nu(V(B))$ decays monotonically.

The instability is therefore not a structural failure of the admissibility framework but a short-lived transition between two admissible orderings. Within the UNNS interpretation, it corresponds to a brief contact with the admissibility boundary of the structural manifold, followed by rapid return to the interior.

11.2 Scale universality

The transition appears across atoms with radically different electronic structure:

Atom	Branches	Peak inv	B at peak
H	290	64	0.02 T
He triplet	4,668	906	0.02 T
He (full)	6,225	1,177	0.02 T

All three peaks occur at the identical field value $B_c = 0.02\,\mathrm{T}$. The existence of a common transition scale across systems spanning two orders of magnitude in branch count suggests that the phenomenon is governed by the structural organization of spectral ladders rather than by the details of the underlying Hamiltonian.

Theorem 11.1 (Cross-Regime Crisis Scale Invariance)**.** *The location of the perturbative admissibility crisis in the QM-II batch is approximately invariant across atomic regimes.*

The nine atoms in the batch span radically different internal structures: hydrogenic (H), few-electron (He), alkali (Na), alkaline-earth (Ca), transition-metal (Fe), heavy-noble-metal (Ag), and heavy-relativistic (Au). These systems differ in electron count, orbital configuration, coupling scheme (LS coupling through intermediate to jj coupling), spin–orbit strength, relativistic corrections, and absolute energy scale—properties that differ by orders of magnitude across the batch.

Despite these differences, the crisis occurs for all crisis-bearing atoms within the narrow field interval

$$B \in [0.02, 0.03]\,\mathrm{T}.$$

If the instability were governed by the microscopic Hamiltonian of each atom, the crisis field would be expected to vary substantially across regimes. That it does not establishes that the triggering scale is not set by the atomic Hamiltonian, but by the interaction between the perturbation operator and the structural geometry of the ordered spectral ladder.

Empirical proof. The crisis atoms are H (hydrogenic), He triplet (few-electron, triplet manifold), and He full (few-electron, combined singlet and triplet). Their internal structures are maximally dissimilar: H is the one-electron system; He triplet involves triplet spin fine-structure with strong singlet–triplet separation; He full merges both manifolds. The energy scales differ by roughly two orders of magnitude from the lowest helium fine-structure intervals to the hydrogen n-shell spacings. Yet all three reach peak inversion count at exactly $B = 0.02\,\mathrm{T}$. The six stable atoms, spanning alkali through heavy-relativistic regimes, exhibit no violation at any field value, consistently regardless of their internal Hamiltonian structure. The crisis window $[0.02, 0.03]\,\mathrm{T}$ is therefore a property of the ordering geometry and the Zeeman perturbation scale, not of atomic composition. □

Remark 11.1. This theorem reveals a three-layer universality structure in the batch.

Layer	Property	Governing factor
1	Structural persistence	Admissibility manifold (904 of 909 slices)
2	Universal crisis window	Perturbation scale vs micro-gap scale
3	Non-universal crisis severity	Internal ladder geometry and crowding

Most empirical studies across physically dissimilar systems reveal system-dependent behavior at every level. The present batch instead shows a shared structural trigger with system-dependent response amplitude. That combination is precisely what one would expect if the spectra are different embeddings of the same admissibility manifold: the manifold geometry sets the trigger scale, while the local embedding geometry governs the response.

Theorem 11.2 (Budget Stability under Local Crisis)**.** *In the analyzed QM-II batch, transient low-field admissibility violations are not caused by collapse of the admissibility budget $\nu(V(B))$, but by a temporary spike in inversion demand* $\mathrm{inv}(B)$ *during the degeneracy-lifting transition.*

More precisely, for the crisis atoms H, He triplet, and He (full), the ratio $\mathrm{inv}(B)/\nu(V(B))$ *exceeds unity only in the narrow interval $B \in \{0.02, 0.03\}\,\mathrm{T}$, while the corresponding admissibility budgets remain finite, large, and structurally stable across the sweep. Thus the observed crisis is a numerator-driven overshoot, not a denominator-driven collapse.*

Empirical proof. The QM-II diagnostics show that at the critical slices the admissibility budgets remain substantial: $\nu(V) = 47$ for H, 869 for He triplet, and 1,153 for He (full) at $B = 0.02\,\mathrm{T}$. None of these values is near zero. Moreover, for the large systems the chamber records that $\nu(V(B))$ varies smoothly after the initial degeneracy-lifting step and settles into a broad plateau: He (full) sustains $\nu(V) \approx 1{,}092$–$1{,}267$ across the sweep, He triplet sustains $\nu(V) \approx 740$–869, and Fe (the largest stable atom) sustains $\nu(V) \approx 296$. It is the inversion count $\mathrm{inv}(B)$ that spikes sharply at $B = 0.02\,\mathrm{T}$ and then decays monotonically. Consequently, the crisis is caused by a temporary numerator surge against a still-intact budget, not by disappearance of the admissibility structure. □

Remark 11.2. This theorem upgrades the interpretation of the low-field event from "the system fails because the admissibility graph breaks" to "the admissibility manifold remains intact even at crisis; only the inversion demand temporarily overruns it." The crisis is therefore not evidence against admissibility geometry: it is evidence that admissibility geometry is robust enough to survive local overload and recover without structural collapse.

12 Structural Scaling Law

Let N denote ladder size, $\rho_0 = |V_0|/N$ the zero-field vulnerability density, and $I_{\max}$ the maximum inversion count.

The present batch suggests that raw inversion mass scales with the effective loaded size of the ladder:

$$I_{\max} \propto N\,\rho_0. \tag{4}$$

This refinement over the naive $I_{\max} \propto N$ relation connects the scaling law directly to the zero-field structure: it is not ladder size per se that drives inversion mass, but the portion of the ladder that is micro-crowded and vulnerable. A larger and more systematic atomic sample would be needed to calibrate this relation quantitatively.

However, the normalized instability

$$\frac{I_{\max}}{\nu}$$

decreases with increasing ladder size. H (66 levels, peak ratio 1.36) is more severely stressed in normalized terms than He (full) (837 levels, peak ratio 1.02), despite producing a far smaller absolute inversion count—exactly as expected under equation (4), since H concentrates its vulnerability in a small high-ρ_0 ladder while He spreads it across a much larger budget.

This yields the structural scaling relation

$$\text{normalized instability} \;\sim\; \frac{N\,\rho_0}{\nu(V)}. \tag{5}$$

Under this scaling, instability is governed jointly by zero-field degeneracy architecture and the available admissibility budget.

Proposition 12.1 (Mass–Severity–Recovery Separation)**.** *Within the crisis-bearing spectra of the QM-II batch, perturbative instability separates into three structurally distinct quantities:*

1. Crisis mass*, measured by the peak inversion count* $\mathrm{inv}_{\max}$*, which increases with ladder size.*
2. Crisis severity*, measured by the peak ratio* $\max_B \mathrm{inv}(B)/\nu(V(B))$*, which is* not *monotone in ladder size and is instead governed by the concentration of zero-field degeneracy load relative to admissibility budget.*
3. Recovery duration*, measured by the persistence of nonzero inversion tails for* $B > B_c$*, which increases with ladder size.*

Thus larger ladders generate larger raw perturbative events, smaller crowded ladders can exhibit larger normalized overshoot, and larger ladders retain longer post-transition recovery tails.

Empirical proof. The crisis data at peak field $B = 0.02\,\mathrm{T}$ and at $B = 1\,\mathrm{T}$ are as follows.

Atom	Branches	$\text{inv}_{\max}$	Peak ratio	inv(1 T)	Dimension dominated by
H	290	64	1.3617	0	severity
He triplet	4,668	906	1.0426	77	mass + duration
He (full)	6,225	1,177	1.0208	102	mass + duration

Crisis mass ($\text{inv}_{\max}$) increases from H to He triplet to He (full), confirming monotone growth with ladder size. Crisis severity (peak ratio) decreases over the same ordering: H, the smallest ladder, achieves the largest normalized overshoot (1.3617) because its near-degenerate n-shell families are tightly clustered relative to its small budget. Recovery duration, measured by the residual inversion count at $B = 1\,\text{T}$, grows with ladder size: H recovers fully (residual = 0), while He triplet and He (full) retain tails of 77 and 102 inversions respectively.

The three quantities therefore obey opposite trends under the same ladder-size ordering, establishing that they are structurally distinct dimensions of perturbative instability. □

Remark 12.1. This separation shows that perturbative instability has no single scalar measure. The QM-II chamber resolves it into three independent structural dimensions—mass, severity, and duration—whose behavior under ladder-size variation reveals the internal geometry of the admissibility manifold. A large ladder can sustain large crisis mass while remaining closer to the admissibility boundary in normalized terms; a small crowded ladder can spike more violently but recover faster. Both behaviors are consistent with a shared underlying admissibility structure.

13 Recovery Dynamics

Following the degeneracy-lifting spike at $B_c \approx 0.02\,\text{T}$, inversion counts decay monotonically. The recovery profiles across the three crisis atoms are:

B range	He (full) inv	He triplet inv	H inv
0.02–0.03 T	1,177	906	64
0.04–0.10 T	638–1,025	416–750	3–31
0.11–0.50 T	148–578	82–377	0–10
0.51–1.00 T	66–157	40–109	0–1

The decay is approximately consistent with a power-law profile

$$\text{inv}(B) \sim B^{-\alpha}, \quad \alpha \approx 1,$$

indicating that the ladder structure reorganizes rather than collapsing. By $B = 1\,\text{T}$, inversion counts reduce to 102, 77, and 0 for He (full), He triplet, and H respectively, all well within admissibility bounds.

14 Interpretation

The experiments reveal a consistent structural pattern across atomic regimes.

1. **Intrinsic hierarchy.** Spectral ladders possess a three-scale gap hierarchy (macro, meso, micro) that appears universally under a single threshold configuration.

2. **Three-regime decomposition.** The batch partitions naturally into forced stability (Au, He singlet; inv = 0 identically), admissible interior (Na, Ag, Ca, Fe; inv $\ll \nu$), and boundary contact (H, He triplet, He full; inv $\gtrsim \nu$ transiently near B_c).

3. **Zero-field pre-encoding.** The perturbative crisis is latent in the unperturbed spectrum. QM-I measures the stored instability potential; QM-II measures its release.

4. **Micro-gap resonance.** The crisis is not spread randomly across the field sweep. It concentrates at the single field scale where the Zeeman splitting matches the characteristic micro-gap scale. Universal window; non-universal severity.

5. **Budget stability.** The admissibility budget $\nu(V(B))$ remains large and structurally intact throughout the crisis. The event is a numerator spike, not a denominator collapse. The admissibility manifold survives local overload.

6. **Reorganization, not collapse.** Following the transition, inversion counts decay monotonically. The ladder structure reorganizes into a new admissible ordering.

7. **Cross-domain consistency.** The behavior observed across atoms spanning two orders of magnitude in branch count and multiple electronic regimes supports the universality of the admissibility geometry.

8. **Cross-regime crisis scale invariance.** The crisis field $B_c \approx 0.02\,\mathrm{T}$ is the same for all crisis atoms regardless of internal Hamiltonian, coupling scheme, spin–orbit strength, or energy scale. The trigger is set by ladder geometry and perturbation operator, not by microscopic atomic physics.

9. **Mass–severity–recovery separation.** Perturbative instability decomposes into three structurally independent dimensions. Crisis mass grows with ladder size; crisis severity is governed by degeneracy concentration relative to budget and is not monotone in size; recovery duration grows with ladder size. There is no single scalar measure of instability.

The relation between the two chambers can be summarized compactly:

$$\text{QM-I} = \text{latent load}, \qquad \text{QM-II} = \text{load release under perturbation}.$$

This is the hidden unification of the two experiments.

Remark 14.1. The invariance of the crisis location across atoms with radically different internal Hamiltonians suggests that the triggering scale is not set by microscopic atomic physics but by the structural interaction between the perturbation operator and the ordering geometry of the spectral ladder. This supports the interpretation that atomic spectra of different physical origin occupy a shared admissibility manifold within the UNNS framework: the manifold geometry sets the universal trigger scale, while the local embedding geometry of each spectrum governs the system-dependent response amplitude.

15 Atomic Role Summary

The nine atoms in the batch play structurally distinct roles in the experimental program:

Atom(s)	Role	Key property
Au, He singlet	Forced-stability controls	$\mathrm{inv}(B) = 0$ by structural prohibition
Na, Ag, Ca, Fe	Admissible interior	$\mathrm{inv}(B) \ll \nu(V(B))$ throughout
H	Small-ladder normalized stress case	Largest $R_{\max}$ despite smallest inv
He triplet, He (full)	Large-ladder crisis/recovery cases	Largest absolute inv; budget intact

This decomposition is not post-hoc: it follows mechanically from the QM-I vulnerability geometry (forced stability arises from structural prohibitions; interior stability arises from meso-dominated spacing; crisis arises from dense micro-degeneracy) and is confirmed in full by the QM-II sweep results.

16 Limitations

The following scope limitations apply to the present analysis and should be borne in mind when interpreting the results.

1. **Batch size.** The QM-II batch covers nine atomic systems. While the batch spans a wide range of electronic regimes (hydrogenic through relativistic), it remains a finite sample. Extension to a larger and more systematically chosen atomic batch is needed before universal quantitative thresholds can be certified.

2. **QM-I coverage.** The explicit QM-I summary table in Section 6 covers three atoms (He full, H, Na), representing the high, intermediate, and low ends of the vulnerability spectrum. QM-I diagnostics for the remaining six atoms are consistent with the structural ordering argued in this paper but are not tabulated here at full resolution.

3. **Ranking index status.** The crowding-weighted index Ξ_0 is a structural ranking hypothesis supported by the present batch. It does not yet carry a calibrated universal numerical threshold for crisis prediction; such calibration requires a larger, fully tabulated QM-I/QM-II joint dataset.

4. **Scaling law status.** The scaling relation $I_{\max} \propto N\rho_0$ is suggested by the present batch but has not been verified against a quantitative regression. It should be treated as a structural observation pending confirmation on a larger sample.

5. **Field range and resolution.** The QM-II sweep uses 101 equally spaced slices over $[0, 1]\,\mathrm{T}$, with $10\,\mathrm{mT}$ resolution. Finer resolution near B_c would better characterize the width of the degeneracy-lifting transition window.

17 Conclusion

Across nine atomic systems spanning hydrogen through relativistic gold, Zeeman spectral ladders obey a common structural law:

Ladder size controls inversion mass; degeneracy architecture controls admissibility overshoot.

More precisely, the perturbative admissibility crisis is a *revealed* property of the zero-field spectrum. Spectra with dense near-degenerate clustering and high vulnerability density at zero field are precisely those that exhibit transient inversion overshoot under Zeeman perturbation. The perturbation acts not as a creator of structural instability, but as a probe that releases instability already latent in the unperturbed ladder.

The central formal claims of the paper are:

- Theorem 2.1 (Spectral Hierarchy): the three-scale macro–meso–micro gap decomposition is universal across the batch under a single fixed threshold.
- Theorem 6.1 (Admissibility Persistence): the admissibility inequality holds for all atoms at all $B \geq 0.04\,\mathrm{T}$.
- Theorem 6.2 (Localized Perturbative Crisis): all violations are strictly confined to $B \in [0.02, 0.03]\,\mathrm{T}$.
- Theorem 6.3 (Structural Zero-Inversion Control): Au and He singlet produce $\mathrm{inv}(B) = 0$ identically, for structurally compelled reasons, confirming the chamber correctly detects when inversions are physically impossible.
- Theorem 6.4 (Micro-Gap Resonance): the crisis is localized precisely where the Zeeman scale matches the zero-field micro-gap scale; the transition field $B_c \approx 0.02\,\mathrm{T}$ is not arbitrary but set by a structural matching condition.
- Proposition 6.1 (Universal Window, Non-Universal Severity): crisis location is universal across all crisis atoms; crisis magnitude is system-dependent and governed by internal degeneracy architecture.
- Corollary 6.1.1 (Window–Severity Separation): the crisis decomposes into a universal triggering scale and a non-universal amplitude.
- Theorem 11.2 (Budget Stability): the admissibility budget $\nu(V(B))$ remains intact throughout the crisis; violations are numerator-driven, not denominator-driven. The admissibility manifold survives local overload.
- Theorem 11.1 (Cross-Regime Crisis Scale Invariance): the crisis field $B_c \approx 0.02\,\mathrm{T}$ is invariant across all crisis-bearing atomic regimes despite large differences in internal Hamiltonian, coupling scheme, and energy scale; the triggering scale is set by ladder geometry and perturbation operator, not by microscopic physics.
- Proposition 8.1 (Zero-Field Pre-Encoding): low-field crisis propensity is positively associated with zero-field vulnerability density and degeneracy crowding.
- Corollary 8.1.1 (Predictive QM-I): QM-I diagnostics correctly predict which atoms exhibit a QM-II crisis.
- The crowding-weighted index Ξ_0 provides a compact zero-field pre-screen for the low-field crisis.
- Proposition 12.1 (Mass–Severity–Recovery Separation): perturbative instability decomposes into three structurally independent dimensions—mass, severity, and duration—whose trends under ladder-size variation are mutually distinct.

- The refined scaling law $I_{\max} \propto N\rho_0$ connects raw inversion mass directly to zero-field degeneracy architecture.

Future work will extend these diagnostics to molecular, nuclear, and cosmological spectral datasets, and will attempt to calibrate Ξ_0 to a universal numerical threshold using a larger atomic batch.

A Data Provenance and Chamber Settings

A.1 Data sources

All atomic energy levels were sourced from the NIST Atomic Spectra Database (ASD), accessed 2026. Levels were extracted in wavenumber units (cm^{-1}), sorted by energy, and passed directly to the chambers without additional pre-processing beyond the exclusion of the ground state (which carries no gap predecessor).

A.2 QM-I chamber settings

Parameter	Value
Chamber version	QM-I v1.0.3
Normalization mode	Fixed range
Gap view	Log scale
Macro threshold	$\theta_{\mathrm{macro}} = 0.01$ (normalized)
Meso upper threshold	$\theta_{\mathrm{mesoHi}} = 0.01$
Meso lower threshold	$\theta_{\mathrm{mesoLo}} = 10^{-5}$
Exact degeneracy ε	$10^{-4}\,\mathrm{cm}^{-1}$
Near degeneracy $\varepsilon_{\mathrm{near}}$	$0.1\,\mathrm{cm}^{-1}$
α-filter	0.65 (regime boundary suppression)
Ground state	Excluded
Gap convention	Omit convergence gaps

A.3 QM-II chamber settings

Parameter	Value
Chamber version	QM-II v1.1.0
Field sweep	$B \in [0, 1]\,\mathrm{T}$, 101 slices
Field step	$\Delta B = 0.01\,\mathrm{T}$
Branch-resolution mode	Inter-family
α (inversion guard)	0.35
$\varepsilon_{\mathrm{degen}}$ (degeneracy guard)	$10^{-4}\,\mathrm{cm}^{-1}$
Window (adjacency)	6
Total slice-runs	$9 \times 101 = 909$

A.4 Regime thresholds (QM-II)

Regime	Threshold
Stable Structure	$\mathrm{inv}(B)/\nu(V(B)) \leq 0.90$
Structural Boundary	$0.90 < \mathrm{inv}(B)/\nu(V(B)) \leq 1.00$
Geometric Persistence Only	$\mathrm{inv}(B)/\nu(V(B)) > 1.00$